

# GBTIDL Calibration and Imaging Tests

## GBT Memo 237

August 19, 2005

Jason Curtis and Glen Langston

### Abstract

This note investigates various calibration techniques with the goal of finding one suitable for producing spectral line and continuum images of Sagittarius B2. We present observations with the GBT in the frequency range 12.4 to 15 GHz (Ku band receiver), of 3C48, J1733-13, and SgrB2. We perform five different calibrations and find that the RMS noise is minimized for the technique that takes the ratio of (Signal - Reference) calibrations on the source, and a reference source. Pointing test results are presented for observations of J1733-13 and 3C48, and are used to determine the intensity conversion from Kelvins to Janskys, and to measure the FWHM beam-width. Finally, two maps are presented as examples of the imaging process that is described in the text.

## 1 Introduction

GBT Observations with the Ku band receiver were made on February 4, 2005, for project TGBT03C\_026. This note presents various calibration techniques with the goal of producing an accurately calibrated map of the Sagittarius B2 molecular cloud, having minimum RMS noise.

Observations were made of 3C48, J1733-13, and Sgr B2. Tipping, peaking, and sub-reflector focusing observations were also made. Section 2 describes the observations made in chronological order. Section 3 describes the various spectral line calibration techniques. Section 4 describes the mapping process in IDL. All tables and figures follow the body of this paper, followed by an appendix of GBTIDL code that may be used to reproduce the results presented in this document.

## 2 Observing Summary

All observations were made on February 4, 2004. The GBT observations are organized into groups of calibrations scans, for determining the antenna pointing accuracy, focus offset and spectral line band pass corrections. Following the calibration scans, the spectral line scans were made to test the spectrometer setup, then followed by 30 mapping scans. Table 2 lists the sources observed, observation type, observing frequency and bandwidth in chronological order.

### 2.1 Hardware Setup and Scan Summary

The system was configured for use of the 12 to 18 GHz front end connected to the GBT spectrometer. Observational parameters are summarized in Table 1. The GBT 12 to 18 GHz front end has two feed horns configured for simultaneous observations of two regions on the sky, offset by 2 arc-min. However, source Sgr B2 has a larger angular extent than the feed separation, so only one feed horn was used for these observations.

The GBT spectrometer was configured for dual polarization, simultaneous observations of four 800 MHz wide spectral bands. The center frequencies of the four spectral bands were 12.8, 13.4, 14.0 and 14.6 GHz, covering the frequency range 12.4 to 15 GHz, with 200 MHz overlap between spectra. The spectrometer was configured for 3 level sampling, with 2048 channels for each spectral band.

During the observations, the noise diode calibration signal (Cal) On/Off switching cycle of 1 Hz was injected into the RF signal path. The noise diode intensity was synchronously detected by the spectrometer during these observations.

## 2.2 Tipping Curve

Observations of the sky temperature versus elevation angle were made at 13.7 GHz. Figure 1 shows the observation in red, and a fit in green. In this case, the observations are approximately fit by an atmospheric attenuation value,  $\tau = 0.014$ , though not very well, due to the higher sky temperature measured toward the galactic center.

## 2.3 Peaking

Peak observations were made on sources J1733-13 (Figure 2) and 3C48 (Figure 3), at 13.7 GHz ( $\lambda = 2.189$  cm) and 13.4835 GHz ( $\lambda = 2.223$  cm) respectively. Based on these observations, we find the GBT FWHM beam width at 13.7 GHz is  $.921 \pm 0.009$  arc-min. At 13.4835 GHz, we find GBT FWHM beam width is  $.933 \pm 0.013$  arc-min.

GBT Memo 232 (Langston et al 2004), performed a similar peaking observation at 9 GHz, and assumed that the FWHM beam width scales with wavelength, giving the equation

$$\theta_A(\lambda) = 0.423 \pm 0.001' \frac{\lambda}{1 \text{ cm}}, \quad (1)$$

where  $\lambda$  is the wavelength in cm. Using our  $\lambda$  values yields beam widths of  $0.926 \pm 0.002$  arc-min, and  $0.94 \pm 0.002$  arc-min, at 13.7 and 13.4835 GHz, which are less than 1% away from our observed values.

## 2.4 Raw Spectra

Nod observations were made on SgrB2 and J1733-13. Figures 6 and 7 show the raw power spectra for each polarization. The dominant noise in the frequency range 12.2→12.7 GHz is due to Satellite T.V. The large spikes in the right circular polarization between 13.6→14.4 GHz are due to problems with the spectrometer.

# 3 Calibration Techniques

We present five calibration techniques, starting with the simplest, and moving on to more sophisticated methods. We will test these techniques on scans 13 → 16, the On/Off Source observations of J1733-13 and Sgr B2. The typical RMS noise for each calibration are listed in Table 3.

## 3.1 Total Power

First, we will perform a total power calibration with the “On Source” observations:

$$T_{ant} = \frac{1}{2} T_{cal} \frac{Cal_{on} + Cal_{off}}{Cal_{on} - Cal_{off}} \quad (2)$$

The resulting spectra are displayed in Figures 8 and 9. The largest spectral fluctuations have been removed, but the spectra are still dominated by noise. Only two potential spectral lines are detectable by visual inspection.

## 3.2 Signal - Reference / Reference

Next, we perform the standard Signal - Reference position calibration:

$$T_{ant} = \frac{Sig - Ref}{Ref} \cdot T_{sys} \quad (3)$$

where *Sig* represents all the spectra on the source, and *Ref* represents all the spectra taken at a location off-set from the source by a few arc-minutes. Both are averaged over all scans, polarizations,

cal. states, and integrations.  $T_{sys}$  is the system temperature. The results are shown in Figures 10 and 11. This calibration reveals many spectral lines, and is sufficient for identifying the majority of the lines, but still contains large scale fluctuations that will prevent successful mapping. Figure 116 overplots the results of this calibration for both SgrB2 and J1733-13. Notice that many of the larger fluctuations are present in both sets of spectra, as well as the large absorption feature near 12.9 GHz.

### 3.3 ...With a Band Pass Correction

We will use the fact that these two very different objects have nearly identical spectral structure, ignoring the lines in SgrB2, to perform the final calibration:

$$S_\nu(\text{Jy}) = \left( \frac{Sig_{SgrB2} - Ref_{SgrB2}}{Ref_{SgrB2}} \right) \cdot \left( \frac{Ref_{J1733-13}}{Sig_{J1733-13} - Ref_{J1733-13}} \right) \cdot S_{J1733-13} \quad (4)$$

where  $S_\nu$  is the flux density of Sgr B2, in Jy. Once again,  $Sig$  is the power spectrum obtained by observing on the source.  $Ref$  is a reference spectrum taken by position switching off the source.  $S_{J1733}$  is a model spectrum, in Jy, for J1733-13. First, a calibrated spectral shape is produced by taking the ratio of a standard signal minus reference over reference calibration for Sgr B2 and J1733-13.

This good, yet relatively simple, line calibration strategy has two sets. The first set is performed setting the GBT RF and IF gains to optimum levels for the target (bright) source and performing observations toward the source and an observation a few arc-minutes offset from the source position.

Computing the ratio of signal ( $Sig$ ) minus reference ( $Ref$ ) and the reference source times the *reference* system temperature  $T_{Ref}$  calibrates the source observation in terms of the observed system temperature of the reference location. Any deviations of the reference position system temperature from the constant value  $T_{Ref}$  appear as features in the  $Sig$  calibrated spectrum.

The second step is measuring these deviations (the band pass correction) determined by observation of the spectrum of a nearly “featureless” radio source, such as a high redshift quasar. For these observations, J1733-13 was observed for computation of the band pass correction. For these band pass observations, the GBT RF and IF gains were set to *different* optimum levels than for the target source observation. The system gain was calibrated by computing the ratio of  $Sig - Ref$  and  $Ref$  scaled by the measured  $T_{RefJ1733}$ , as show by equation 4.

Our observations of these two very different sources have nearly identical spectral structure, ignoring the lines in Sgr B2. This is clearly an artifact of the GBT RF and IF gain as a function of frequency, not the spectral properties of these two sources. Computing this ratio calibrates the band pass spectrum. Note that this quantity produces a calibrated shape for our power spectrum, but is dimensionless. We therefore scale this shape by  $S(\nu)$ , a model spectrum for J1733-13, with flux density in Jy. J1733-13 is a compact radio source, whose spectrum should appear to us featureless and approximately flat. This means we can model it by generating a flat spectrum at the observed flux density in Jy.

$$S_{J1733-13}(\nu) = \frac{S_{J1733-13}(\nu = 13.7)}{S_{3C48}(\nu = 13.48)} \cdot S_{3C48}(\nu) \quad (5)$$

This model is generated with the flux density value at  $\nu=13.7$  GHz. where  $S_{J1733-13}(\nu = 13.7)$  is the continuum intensity of J1733-13 at  $\nu = 13.7GHz$ , and  $S_{3C48}(\nu = 13.48)$  is the continuum intensity of 3C48 at  $\nu = 13.48GHz$ . These two intensities were measured from the averaged gaussian heights of the four peaking observations, and yield values of 11.05 and 2.40 for J1733-13 and 3C48. (See Figures 2→5)

Ott et. al 1994 provides a model for the flux density, in Jy, for 3C48:

$$\log(S_{3C48}) = a + b \cdot \log(\nu) + c \cdot \log(\nu)^2 \quad (6)$$

with  $\mathbf{a= 2.465}$ ,  $\mathbf{b= -.004}$ ,  $\mathbf{c= -.1251}$ , for frequencies ranging from 1408 MHz  $\rightarrow$  23780 MHz. We find 9.51 Jy for the flux density of J1733-13, at  $\nu=13.7$  GHz.

Because of the frequency dependence of the RF and IF gain, the calibrated spectra from each of the four bands do not line up. Above, we noted that each spectral band has a 200 MHz overlap with the next (See Figure 13: the overplot of the calibrated spectra from bands 1 and 2, averaged over polarization). We can use overlapping  $H\alpha$  lines as a reference, and align all the spectra in

reference to the 13.7 GHz position. Figure 12 shows the calibrated spectra from all four spectral bands, in both polarizations (the Red line is left circular, and Black is right circular). As you can see, the large absorption feature near 12.9 GHz is actually an artifact of our system, and not of astronomical origin.

### 3.4 ...And Modified a Bit

Dividing each  $Sig - Ref$  in equation 4, by  $Ref$ , is necessary when the attenuation is changed between the observations of the different sources. This attenuation may be changed to optimize the functioning of the spectrometer. Dividing by this  $Ref$  term does introduce a tiny amount of noise compared with:

$$S_{\nu}(Jy) = \left( \frac{(Sig - Ref)_{SgrB2}}{(Sig - Ref)_{J1733-13}} \right) \cdot S_{J1733-13} \quad (7)$$

but does not yield the best calibrated flux density. The noise introduced is less than a 1 % effect, and therefore does practically nothing to clean up the spectra anyway.

### 3.5 ...With Median Subtraction

We are currently preparing a paper (Langston and Curtis 2005) presenting our work with SgrB2. Included in this paper, is a discussion on the process of Median Subtraction. We refer the reader to this concurrent paper, and will only briefly describe the process here, and present a plot (Figure 6 comparing spectra calibrated with and without median subtraction.

Briefly, median subtraction does this and that...

## 4 Imaging in IDL

Our observations of Sgr B2 covered the  $10^{\circ} \times 10^{\circ}$  angular region,  $8^h 32^m < \alpha < 11^h 00^m 51^s$  and  $65^d < \delta < 74^d$  (J2000). The above calibration was performed on Nod data, with the reference being the observation of a position, offset by a few arc-minutes from the center of Sgr B2. This offset position lies within the extended emission of the cloud. In such a situation, it is common to extend the mapping region, and average the spectra along the borders of the map. In our situation, the bottom half of the map is not “free” of continuum emission, and performing such an average would contaminate the calibration. Instead, a pixel, at the position of minimum continuum emission, was chosen for the reference position. This will provide the best calibration for the map. Next, gaussians are fit to each line. The peak height is taken as the peak flux density at that position, and the intensity is inserted into an array.

With the aid of (Heiles 2004), we have written two procedures in IDL (`display`, `display_ps`) that take this array, and produce an image from it. Our procedure makes use of the already existing `tvsc1` procedure and `congrid` function, as well as Tim Robishaw’s `psopen` and `psclose` procedures for producing postscript files, and extend these to provide the capability to completely annotate the image with plot border and labels, an intensity reference bar, contours of any desired transition, and a contour at .5 Jy of the response of our beam to a model 1 Jy source. Figures 19 and 20 are included to demonstrate the capabilities of our imaging procedures.

## 5 Summary

We find it necessary, particularly in our observations with such a large bandwidth, to not only perform position-switched observations on the source of interest, in our case, Sagittarius B2, but also perform similar observations on a nearby compact radio source that can be used to compute a band pass correction. Performing either calibration from Sections 3.3 and 3.4 sufficiently reduce the rms noise. If the reference source does not have a well-known flux-density over the required frequency range, then peaking observations of such a known source, like 3C48, can be used to determine the intensity conversion from Kelvins to Janskys.

The optimum calibration technique for reducing Nod data can also be applied, with a simple modification, to mapping observations. We have developed a series of GBTIDL procedures and

functions that calibrate mapping data, fit gaussians to the spectral lines, and produce R.A.-Dec. maps at the specified transition. These maps are automatically labeled, equipped with a flux density reference bar, allow for contours to be overlaid at any desired transition, with a postscript copy available on command. These procedures and functions, with some work, could be modified and adapted into GBTIDL to allow for easier production of high-quality images.

## 6 References

1. Heiles, C. (2004), "BIDIDL: Basic Image Display in IDL"
2. Langston, G., Braatz, J., Ghigo, F., Maddalena, R., Minter, T., and O'Neal, K. (2005), "GBT Memo 232: Apparent Temperature of Mercury, Mars, Saturn, and Venus at X Band"
3. Langston, G., and Curtis, J. (2005), in preparation.
4. Ott, M. Witzel, A., Quirrenbach, A., Kirchbaum, T.P. Standke, K., J., Schalinski, C. J., and Hummel, C.A., (1994) *Astronomy and Astrophysics*, Vol 284 pg 331.

Telescope:	
Diameter.....	100 m
Beamwidth .....	0.921 at 13.7 GHz
Linear resolution .....	$2.3 \frac{D}{8.5 kpc} pc$
Aperture efficiency .....	$\sim 0.69$
Receiver:	
System Temperature .....	$\sim 30$ K
Spectrometer:	
Bandwidth.....	4x800 MHz
Resolution, Hanning Smoothed.....	0.39 MHz (8.6 km s <sup>-1</sup> )
Speed of Mapping:	
Time to cover 10 × 10...	$\sim 2$ hours

Table 1: Parameters of the Robert C. Byrd Green Bank Telescope System

Start Scan	Stop Scan	Object	Scan Type	RA-2000 (hms)	Dec-2000 (d <sup>m</sup> )	Frequency (MHz)	Bandwidth (MHz)	Start Time (UTC)
1	1	Tipping	Tipping	14h38m28	6d36'20	13700.000	80.0	13:02:57
2	3	J1733-13	Nod	17h33m03	-13d04'49	12801.061	800.0	13:15:06
4	7	J1733-13	Peak	17h33m03	-13d04'49	13700.000	80.0	13:18:52
8	8	J1733-13	FocusSubreflec	17h33m03	-13d04'49	13700.000	80.0	13:21:13
9	9	J1733-13	FocusSubreflec	17h33m03	-13d04'49	13700.000	3500.0	13:26:11
10	11	J1733-13	Nod	17h33m03	-13d04'49	12800.000	800.0	13:28:53
12	12	J1733-13	Track	17h33m03	-13d04'49	12800.000	800.0	13:32:30
13	14	J1733-13	Nod	17h33m03	-13d04'49	12800.000	800.0	13:35:10
15	16	SGRB2	Nod	17h47m20	-28d23'07	12800.000	800.0	13:37:58
17	46	SGRB2	RALongMap	17h47m20	-28d18'17	12800.000	800.0	13:45:24
47	48	SGRB2	Nod	17h47m20	-28d23'07	13530.990	12.5	14:47:36
49	50	SGRB2	Nod	17h47m20	-28d23'07	13530.990	12.5	14:51:31
51	54	3C48	Peak	1h37m41	33d09'35	13483.500	320.0	14:57:50
55	55	3C48	FocusSubreflec	1h37m41	33d09'36	13483.500	320.0	14:59:53
56	57	3C48	Nod	1h37m41	33d09'36	13530.000	12.5	15:03:46

Table 2: Scan Summary of Ku band observations on 2004 Feb 4. This observing summary was produced using the validator program.

Calibration Technique	Typical RMS Noise (Jy)
Total Power	.1482
(Sig-Ref)/Ref	.1182
[(Sig-Ref/Ref) <sub>1</sub> / [(Sig-Ref)/Ref] <sub>2</sub>	.0281
[Sig-Ref] <sub>1</sub> / [Sig-Ref] <sub>2</sub>	.0279
Median Subtraction	.0280

Table 3: Typical rms noise for various calibrations. Polarizations were averaged. Four samples were taken, one in each band, and averaged.

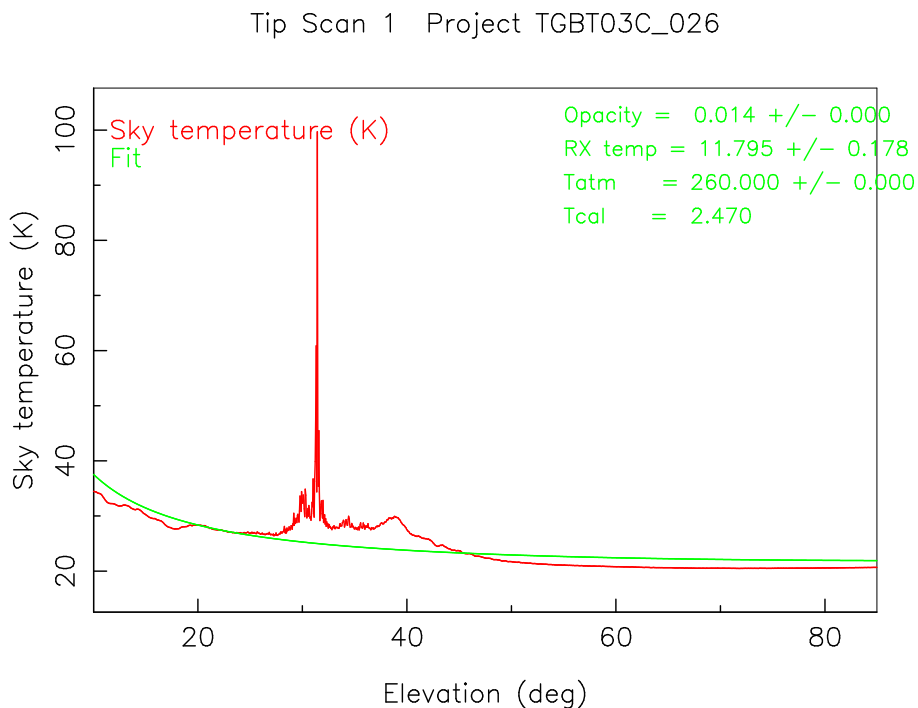


Figure 1: Tipping observations at 13.7 GHz fit to a secant( $z$ ) opacity model, where  $T_{atmosphere} = 260$  is assumed.

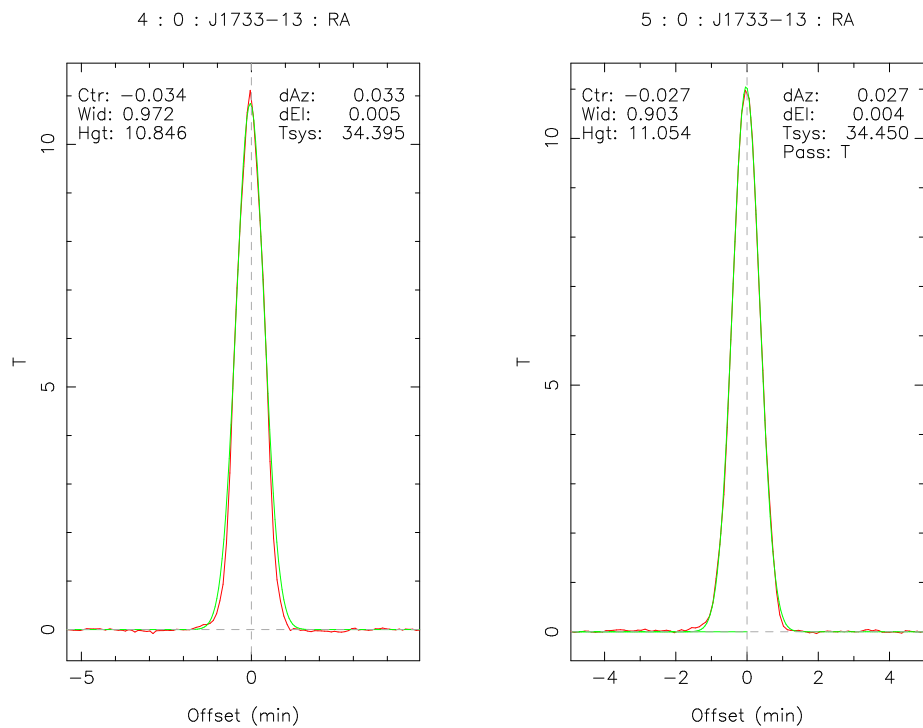


Figure 2: Pair of Peak scans in the RA direction towards J1733-13.

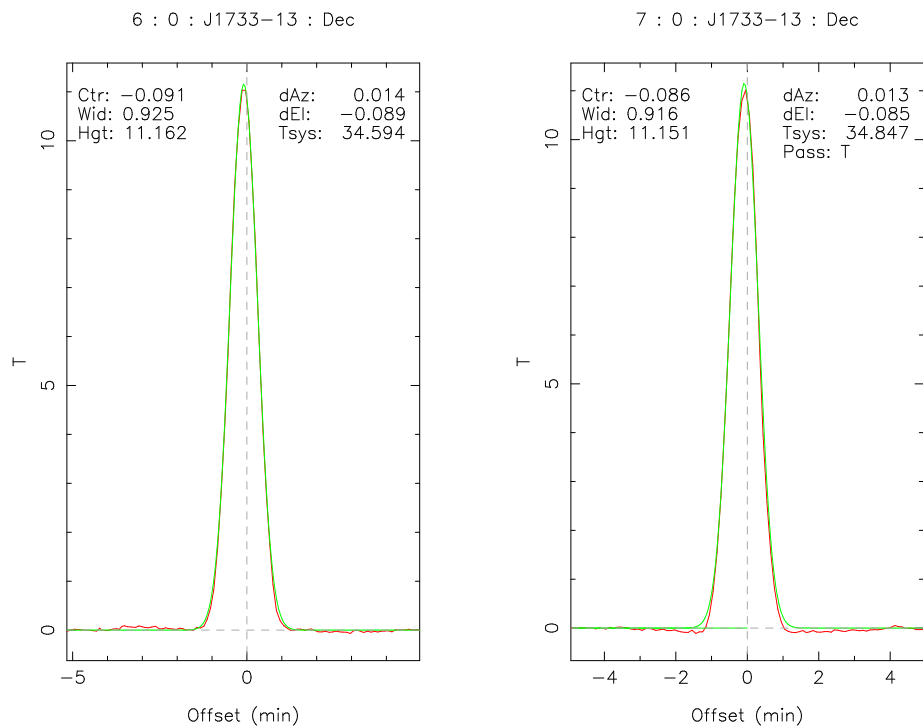


Figure 3: Pair of Peak scans in the Dec direction towards J1733-13 .

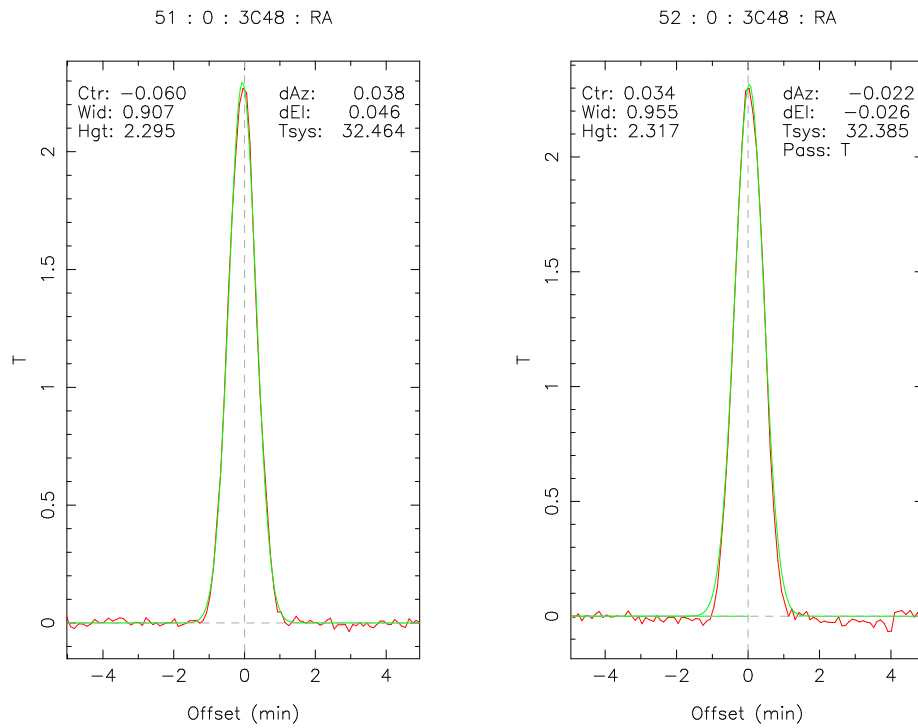


Figure 4: Pair of Peak scans in the RA direction towards 3C48.

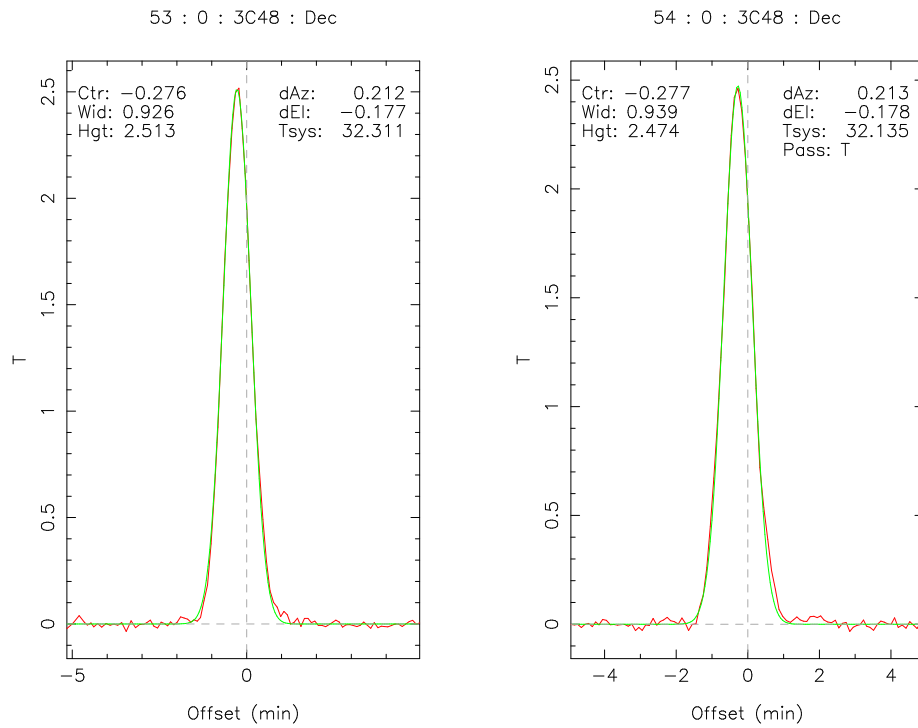


Figure 5: Pair of Peak scans in the Dec direction towards 3C48.

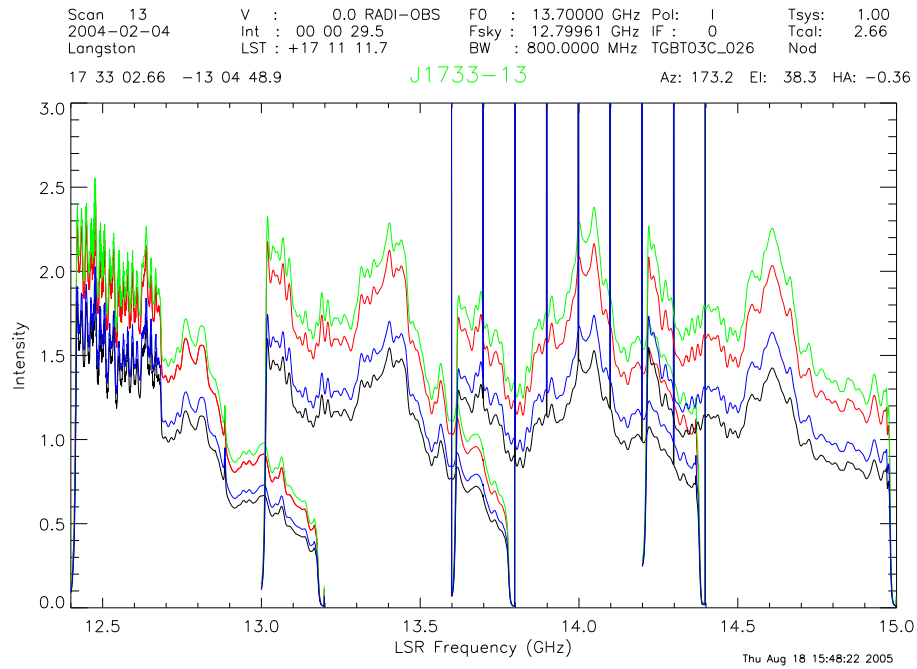


Figure 6: J1733-13: Raw, uncalibrated data. Intensity versus frequency plot in four 800MHz banks. Green line: On Source, Cal On. Red line: On Source, Cal Off. Blue line: Off Source, Cal On. Black line: Off Source, Cal Off

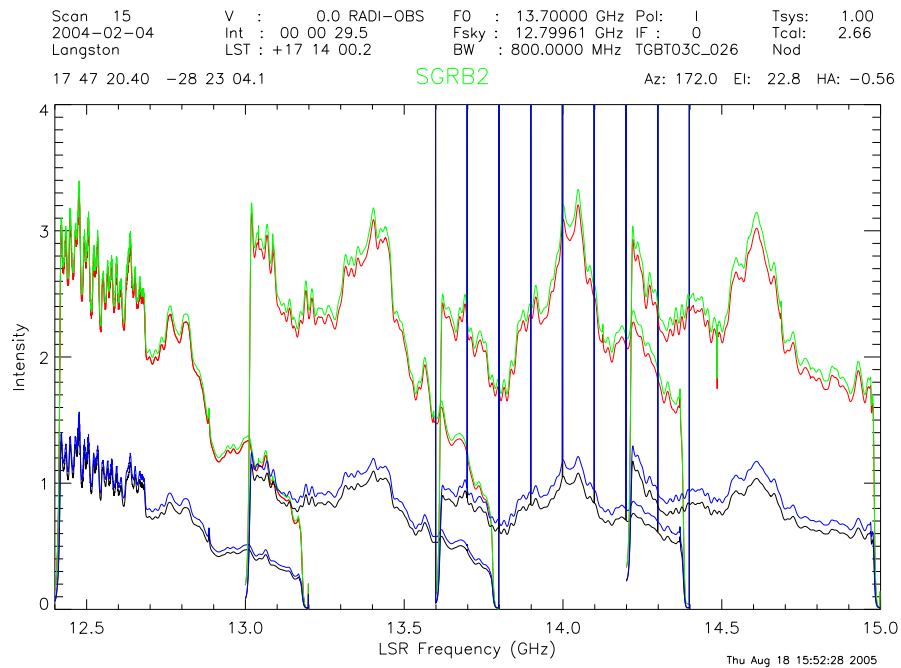


Figure 7: SgrB2: Raw, uncalibrated data. Intensity versus frequency plot in four 800MHz banks. Green line: On Source, Cal On. Red line: On Source, Cal Off. Blue line: Off Source, Cal On. Black line: Off Source, Cal Off

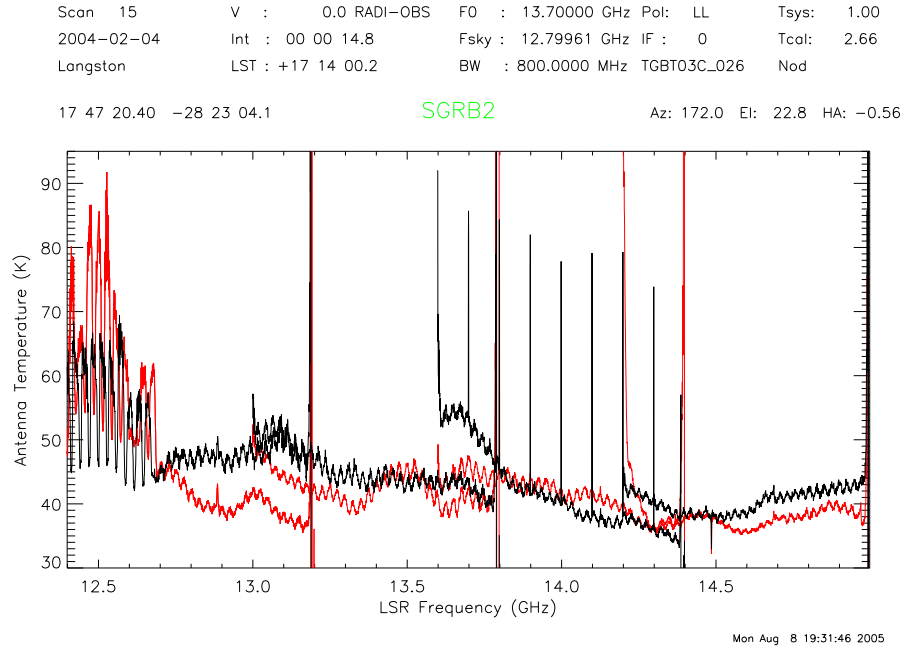


Figure 8: First Calibration: Antenna Temperature versus frequency plot for four scans towards J1733-13. The antenna temperature is calibrated by measurement of the calibration noise diode intensity, which is toggle on and off at a 1 Hz rate during the observations.

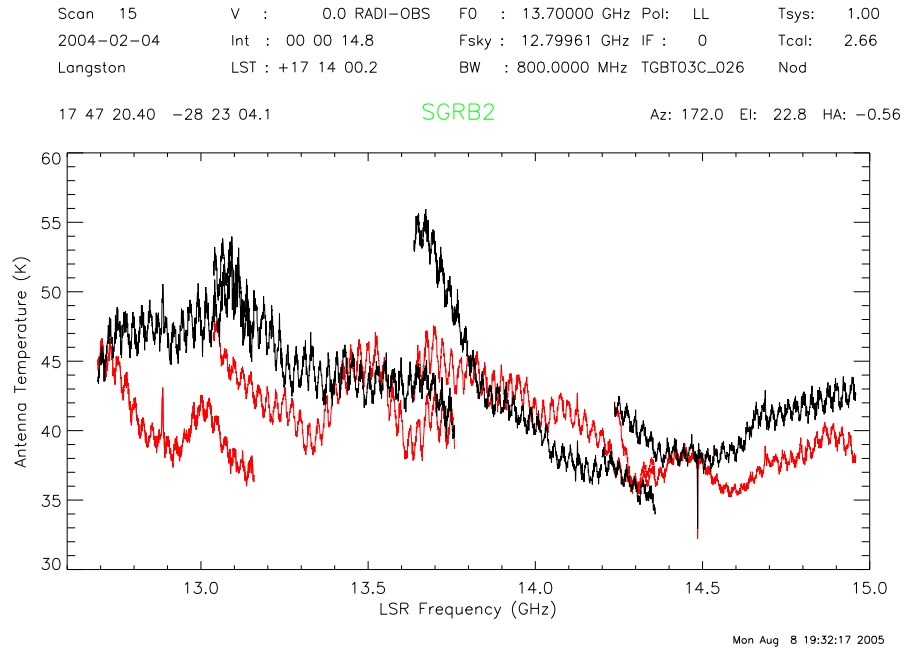


Figure 9: First Calibration: Antenna Temperature versus frequency plot for four scans towards SgrB2. The antenna temperature is calibrated by measurement of the calibration noise diode intensity, which is toggle on and off at a 1 Hz rate during the observations.

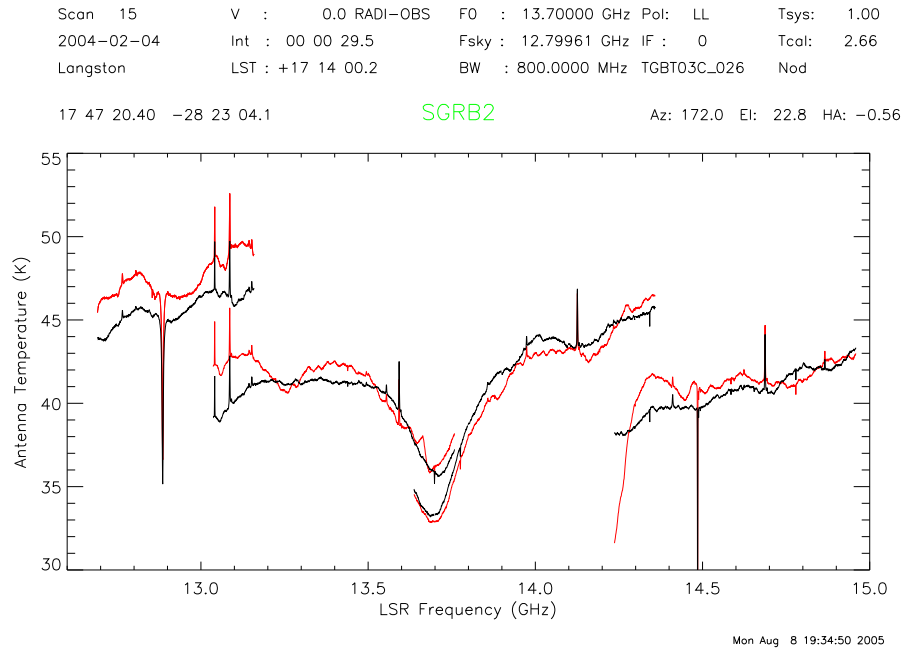


Figure 10: First Calibration: Antenna Temperature versus frequency plot for four scans towards J1733-13. The antenna temperature is calibrated by measurement of the calibration noise diode intensity, which is toggle on and off at a 1 Hz rate during the observations.

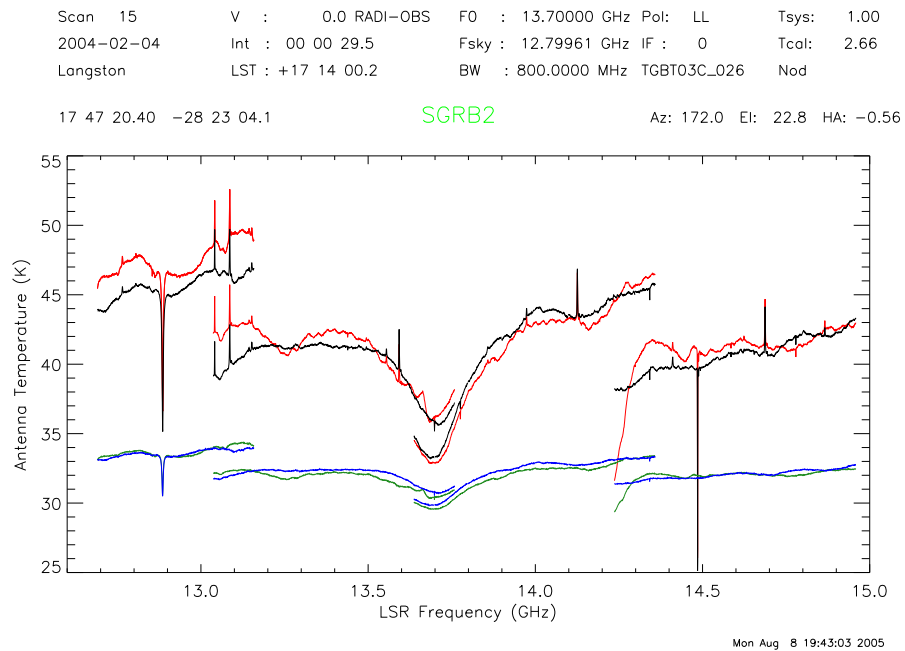
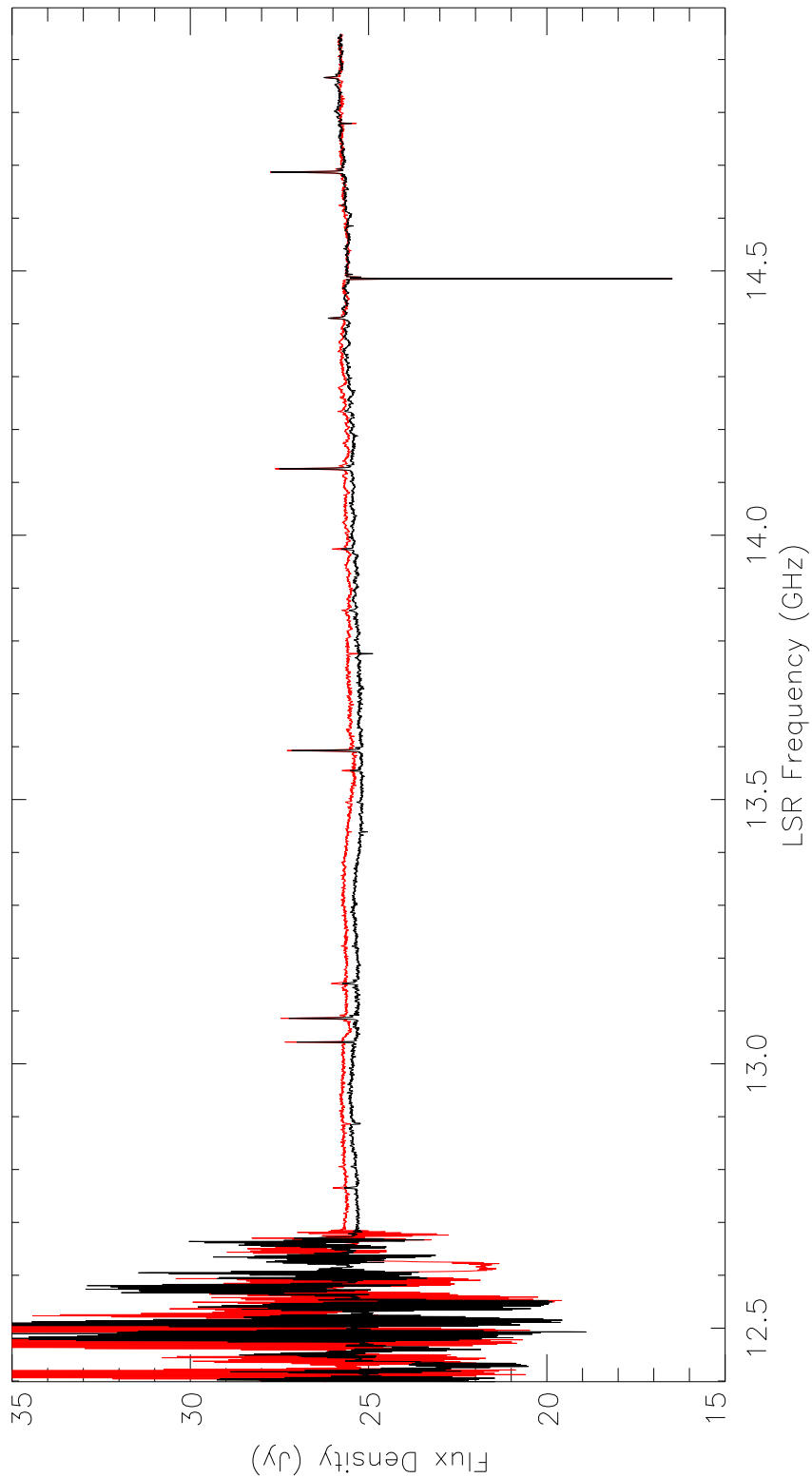


Figure 11: First Calibration: Antenna Temperature versus frequency plot for four scans towards SgrB2. The antenna temperature is calibrated by measurement of the calibration noise diode intensity, which is toggle on and off at a 1 Hz rate during the observations.

Scan 15 V : -62.0 RAD1-OBS F0 : 13.70000 GHz Pol: LL Tsys: 28.03  
 2004-02-04 Int : 00 00 29.5 Fsky : 12.79961 GHz IF : 0 Tcdl: 2.66  
 Langston LST : +17 14 00.2 BW : 800.0000 MHz TGBT03C\_026 Nod  
 17 47 20.40 -28 23 04.1 **SGRB2** Az: 172.0 El: 22.8 HA: -0.56



Tue Aug 9 11:47:44 2005

Figure 12: Plot of intensity versus frequency for the 4 spectral bands observed simultaneously. Red: Left circular polarization. Black: Right circular polarization



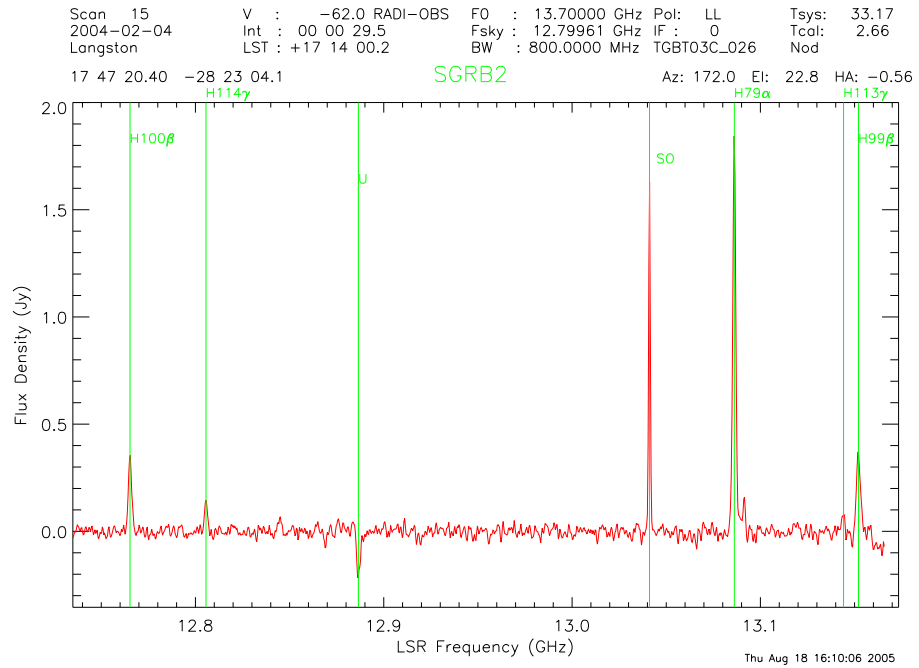


Figure 15: Calibrated Spectrum of first band

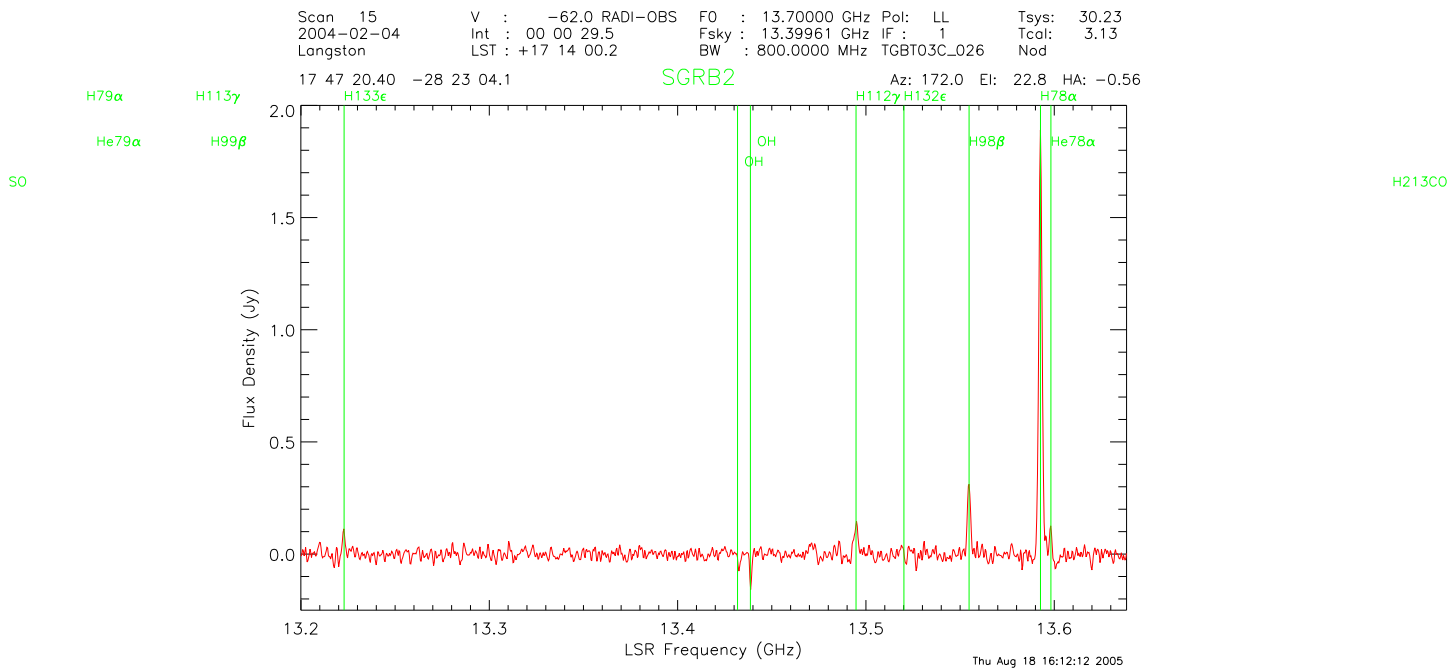


Figure 16: Calibrated Spectrum of second band

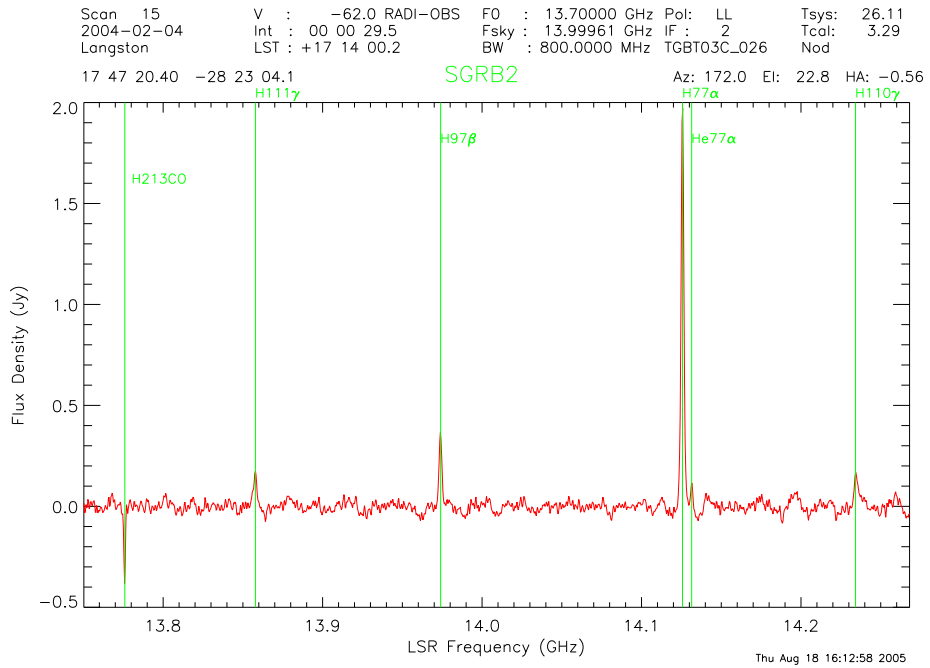


Figure 17: Calibrated Spectrum of third band

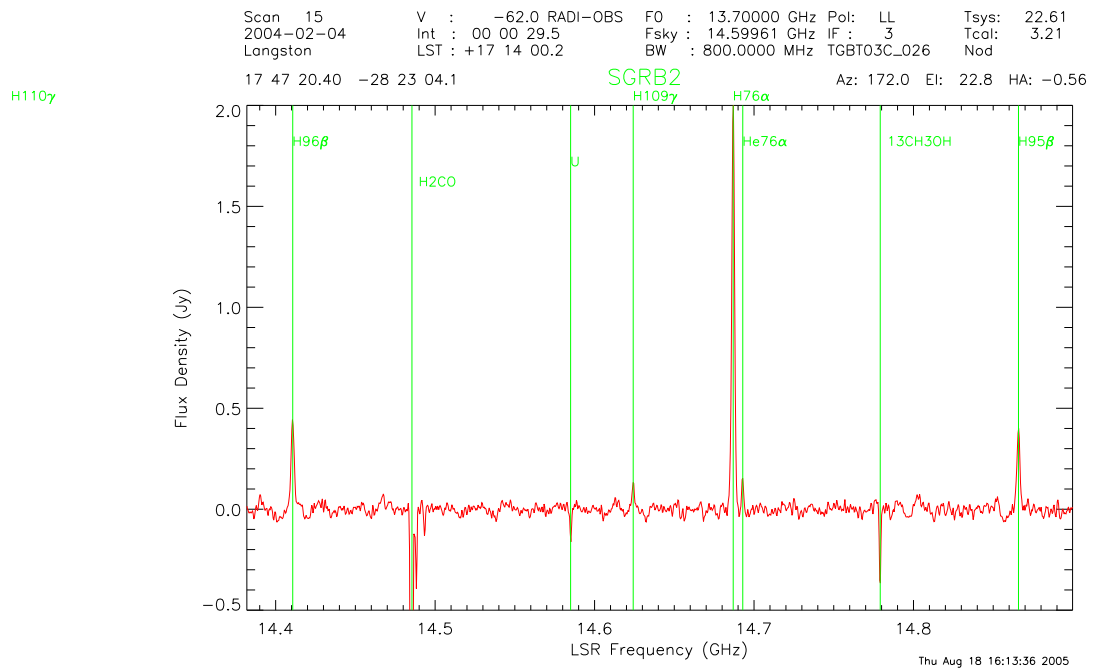


Figure 18: Calibrated Spectrum of fourth band

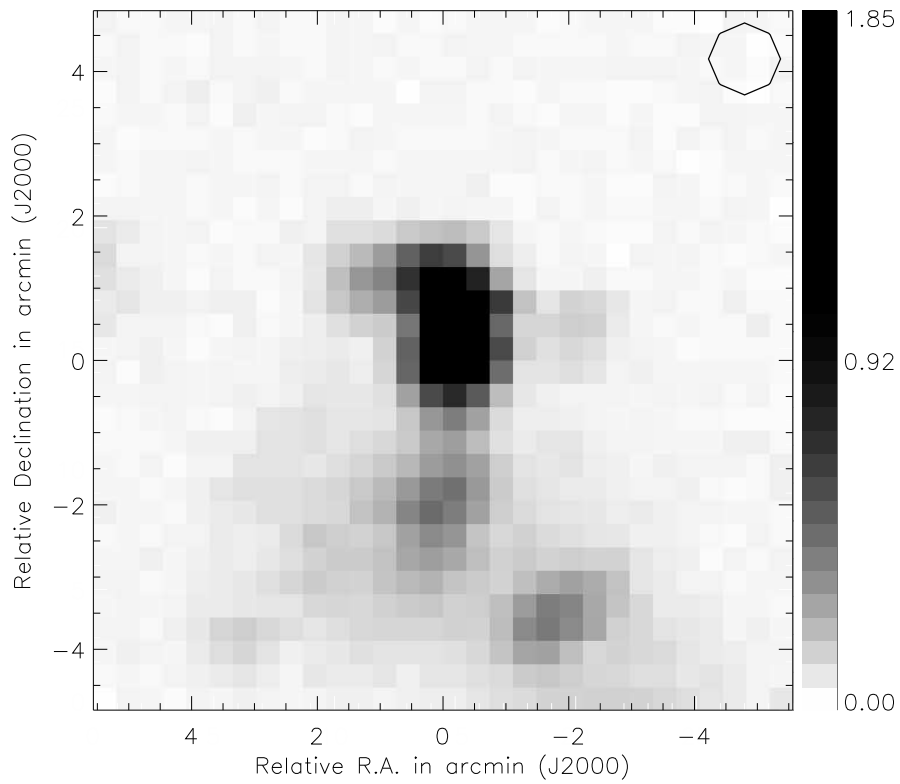


Figure 19: Map: grayscale image of averaged H $\alpha$  76 $\rightarrow$ 79 emission (Jy). Top-right corner: Our beam response to a model 1Jy source. Contour at .5 Jy.

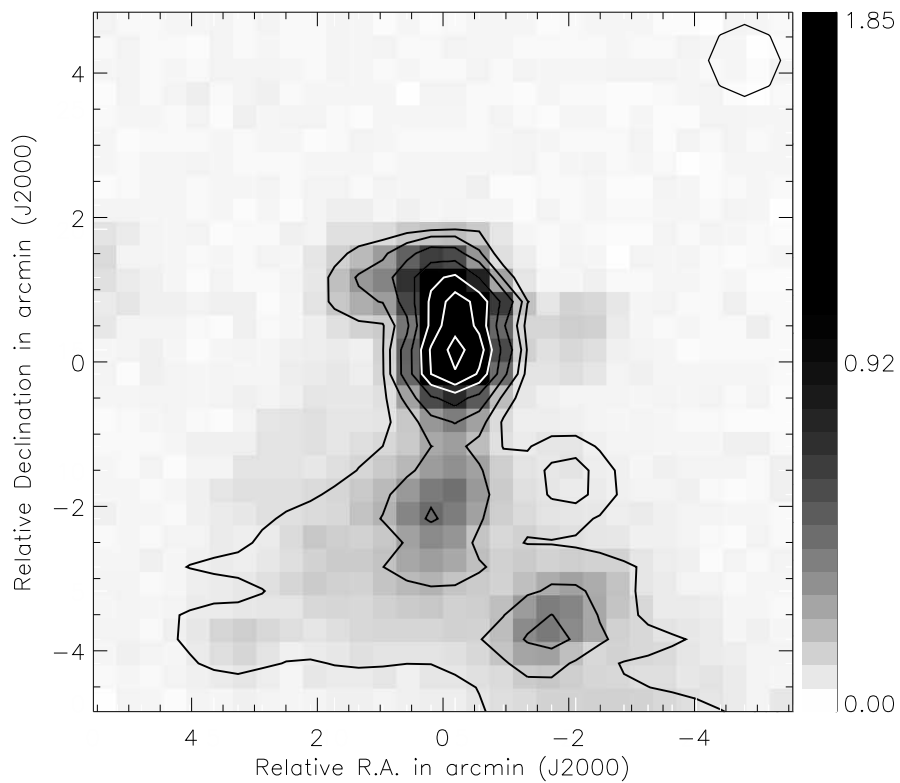


Figure 20: Map with Contours: grayscale image of averaged H $\alpha$  76 $\rightarrow$ 79 emission, with 14440 MHz continuum emission contours overlaid at 5, 10, 20, 33, 50, 66, and 90 percent of peak flux density.

## A Overview of GBTIDL Procedures and Functions

In the main body of this memo, I have discussed the general principles involved in the calibration of Nod data and producing quality images. Here, I will discuss in more detail *how* to do this in GBTIDL, and include a list and description of our procedures and functions. The code can currently be found locally at `/jcurtis/Jason2005/` or `/glangsto/???`

## B Display

Imaging in IDL is pretty straightforward. Everything is already built into IDL. What makes `display` unique and powerful, is that it pulls all the different parts together in one package. `congrid` is used to enlarge the image, which is so needed in our case, as our image is 30x30 pixels. `tv` does a great job of turning an array of intensities into a picture. `can` can be used to scale the intensities into the byte value range 0→255. `xloadct` can be used quite effectively for altering the color table to bring out weaker features. Annotating the plot with labels and units can be trickier, and I strongly suggest Carl Heiles' *BIBIDL* paper for a fuller discussion. The first step is to create a window that is larger than the size of the image. The image can now be generated in the center of this window. Next, `plot` is used to generate an axis on top of the image, without any data, and with x- and y-value arrays, and labels laid down. To create a reference bar, an array, ranging from the minimum to the maximum of the byte-scaled intensity array, is created and imaged next to the main plot. An axis can be created the same as it was for the image, and `axis` is used to customize and turn off unwanted axes. Contours can be overlaid with `contour`. A contour at .5 Jy of the beam response to a model 1 Jy source is overlaid in the top-right corner. `display_ps` (`disp_ps.pro`) does the same thing as `display`, but some things need to be tweaked to get the postscript to come out right.

## C Calibration of Nod Data

The calibration is run through our `calib.pro` procedure. We take advantage of the GBTIDL global structure spectral line data container, and the basic `add`, `subtract`, `divide` procedures to perform the calculation. The `stack` is useful for selecting and averaging particular spectra. For example, for the *Sig*, we select all spectra that have a particular scan number, polarization, and spectral index. All spectra that meet these criteria are selected out and averaged.

Within `calib`, there are four sub-programs that are called on. `J1733model.func` calculates the flux density of J1733-13, in Jy, with the ratio of the peaking observations on this source and 3C48, and scales this ratio by the flux density of 3C48 according to Ott et.al 1994.

`fixspecLL.pro` and `fixspecRR.pro` perform the alignment of the four spectral bands, and flag out overlapping regions, and the satellite TV interference. `fixspecRR.pro` also crops out the spikes from the faulty spectrometer.

`calib_tsys.pro` calculates the system temperature, and saves this value into the header in the calibrated spectra data containers.

## D Mapping

The mapping is run by `map.pro`. This procedure loads two data files, `axis.sav` and `fitline.sav`. `axis.sav` was generated with `locations.pro` (do not try this at home), which looked through all 14400 spectra, and selected out the maximum and minimum R.A. and Declination values to be used to label the map axes. `fitline.sav` was generated with the function `fitline.func`, which creates a structure that contains information about all the spectral lines. It does this by allowing the user to select a region around a line, and then it calculates an estimate for the four gaussian parameters, height, center frequency, line width, and continuum strength. The height is estimated by calculating the peak (maximum for emission, minimum for absorption) within the specified range, and subtracting off the median value for that range. This median is taken as the continuum strength. The center frequency is taken as the frequency that corresponds to this peak. And the line width is estimated by stepping down the peak (or up the trough for absorption), until a change in concavity is located. The gaussian, and its parameters, are stored into the structure, and are

used to calculate the LSR frequency, radial velocity, velocity width, and the uncertainties associated with these values.

Back to `map.pro`, the R.A. and Dec values are converted into units of relative arcminutes. Next, either `map_mapping.func` or `map_continuum.func` will be loaded, depending on whether you wish to map spectral lines or continuum emission. An array of intensities is returned and passed to `display.pro` which will produce an image of the map.

Both of the mapping tools take advantage of `map_calib.pro`. This procedure performs the same calibration described in the above section, as well as in Section 3.3. The only difference is the reference location for SgrB2 is taken as the point of minimum continuum, instead of the arbitrary Nod offset, which actually falls within the extended emission of the cloud.

`map_continuum.func` sets up this calibration, and loops through R.A. integrations and Declination scans, performs the calibration at each point, and then calculates the continuum flux density by taking the median of a region free of spectral lines. These intensities are inserted into an intensity array that is, once again, passed back to `map.pro` and into `display.pro`.

`map_mapping.func` also performs the calibration with `map_calib.pro`, but then the calibrated spectra are passed to `map_gauss.func`, which fits a gaussian to the requested line in a manner very similar to `fitline.func`. The boundary for the gaussian is set by selecting a region in velocity space that surrounds the value found in the `fitline` structure. The region of velocity coverage is not a parameter of this function, but can be altered in the code to widen or narrow the region. Once estimates are made, and the gaussian fitted, `map_gauss.func` calls on a verification procedure, `map_emission.pro` for emission lines and `map_absorp.pro` for absorption lines, which subjects the fit to a series of tests. Normally, the fitting works fine, but in the case where there is no detectable signal, just noise, then a gaussian is occasionally fit with a height of 10 million, or a negative width, or some other obviously wrong and wild value. When this is the case, the fitted height is rejected and the difference between the peak intensity within the bounds, and an averaged continuum value is taken as the intensity. This is done in place of setting the intensity to zero, because it allows the map to retain a background noise. After suitable intensity values are calculated, these values are passed to `map_image.func`, which stores them in an array, and returns this array back to the `map_mapping` level. This array, along with a structure named `linefit` containing the fitting parameters and errors at each point, is saved with the filename: 'line name'.sav. And, again, this image array is passed back to `map.pro` and into `display.pro`, where an image is generated on the screen.

Once a map is generated for each line, there is no need to keep running this procedure to redisplay the map. Instead, we have a useful procedure, `showmap.pro`, which enables users to display an already existing map file, and has the option of overlaying contours of any line or continuum emission. `showmap.pro` also has a keyword that allows a postscript version to be created.

The beam response pattern that was described above in the Display section, was generated with the procedure, `map_beam.pro`. This takes a 1 Jy source, and computes how it responds to a gaussian with a FWHM equal to that of our beam, and at a distance equal to the radial distance from the central peak.